EES Solar

PAPER

View Article Online
View Journal | View Issue

Open Access Article. Published on 21 January 2025. Downloaded on 1/22/2026 1:24:09 AM.
This article is licensed under a Creative Commons Attribution-NonCommercial 3.0 Unported Licence.

Check for updates

Cite this: *EES Sol.*, 2025, **1**, 172

Thermal and photodegradation mechanism of (FA-MA)PbI$_3$ perovskite and spiro-OMeTAD captured by *in situ* EPR spectroscopy†

Julie Ruellou,[a] Hania Ahouari,[b] Matthieu Courty,[a] Hervé Vezin[b] and Frédéric Sauvage *[a]

Received 10th September 2024
Accepted 25th December 2024

DOI: 10.1039/d4el00003j

rsc.li/EESSolar

A comprehensive description of halide perovskite degradation is still lacking. Light and temperature are herein combined as stressors to gain novel insights into the involvement of free carriers in the degradation of $(FA_{0.73}MA_{0.27})Pb(I_{0.945}Br_{0.055})_3$ and spiro-OMeTAD. *In situ* EPR spectroscopy is at the core of this study because of its ability to probe free carriers with high sensitivity. The results are corroborated with *in situ* X-ray diffraction, and thermogravimetric and calorimetric analysis to link the generation of free carriers with long-range structural modification, gas release and heat exchange during degradation. It is highlighted that temperature-induced perovskite decomposition does not involve radicals, in contrast to the final stage of the decomposition, which involves radicals localized on the formamidinium. When combined with light, the rise in spin concentration correlates with the increasing rate of the degradation compared to that in darkness. The de-doping reaction of spiro-OMeTAD is observed up to its crystallisation temperature (128 °C). Finally, by combining light, temperature and an external magnetic field, we provide the first evaluation of the room-temperature exciton binding energy for $(FA_{0.73}MA_{0.27})Pb(I_{0.945}Br_{0.055})_3$, for which a value of 43 meV was determined.

Broader context

Halide perovskite materials have significant potential to revolutionize various fields related to optoelectronics, in particular for photovoltaics for which a never before reached level of performance has now been achieved. The main attributes of these materials stem from a combination of unique photophysical properties and the richness of the composition space, which overall can be adapted to specific needs. However, significant challenges in achieving long-term stability remain to fully capitalize on the efforts in material development and properties. To capture degradation mechanisms, it is important to combine very sensitive techniques to probe the seeds, correlated with tools sensitive to the long-range, together with an *in situ* approach to reveal in real time the failure mechanisms without having to stop the ageing and characterization of the event under non-stressing conditions. In this work, we combine different techniques and provide a correlative dataset through *in situ* electron spin resonance to assess the involvement of free carriers, *in situ* X-ray diffraction to link carriers to structural degradation and a thermogravimetric/calorimetric approach combined with mass spectrometry to obtain additional information regarding formation of volatile compounds and heat exchange during degradation. This study reveals in real time the involvement of the free carriers generated in α-FAPbI$_3$ and spiro-OMeTAD upon temperature and light. New insights are provided on the step-by-step breakdown of the perovskite and spiro-OMeTAD materials when exposed to temperature and when combined with light as an additional stressor. This approach provides crucial insights for the community focusing on strengthening perovskite materials, interfaces and overall stack stability.

Introduction

Significant achievements have been made in raising hybrid halide perovskite performance, mainly through molecular passivation of non-radiative electronic defects, composition engineering and interface control. These unprecedented efforts have reinforced the credible idea that perovskite technology will be at the forefront of thin-film photovoltaics. Today, power conversion efficiencies (PCEs) of 26.7% in laboratory cells, 18.6% in small modules (810 cm^2) and 34.5% in monolithic materials (2 terminal) in tandem with Si (1 cm^2 active area) have been reported.[1,2] One important asset of perovskites lies in the vast chemical richness offered by the possibility of combining different monovalent cations, including organics in the A site,[3] potentially mixing lead with tin, bismuth or other elements in the B site,[4] and finally through anionic substitution with halides or pseudo-halides.[5] This wide range from simple to more complex intermixing of elements contributes to an almost endless composition space, which not only enables fine optical

[a]*Laboratoire de Réactivité et Chimie des Solides, CNRS UMR7314, Université de Picardie Jules Verne, Hub de l'énergie, 15 Rue Baudelocque, 80039 Amiens Cedex, France. E-mail: frederic.sauvage@u-picardie.fr*

[b]*LASIRE – Laboratoire Avancé de Spectroscopie pour les Interactions la Réactivité et l'Environnement, CNRS UMR 8516, University of Lille, F-59000 Lille, France*

† Electronic supplementary information (ESI) available. See DOI: https://doi.org/10.1039/d4el00003j

© 2025 The Author(s). Published by the Royal Society of Chemistry

Open Access Article. Published on 21 January 2025. Downloaded on 1/22/2026 1:24:09 AM.
This article is licensed under a Creative Commons Attribution-NonCommercial 3.0 Unported Licence.

bandgap control[6] but also extends the range of functional physical properties more globally. Perovskites gather a unique combination of physical attributes, such as structural softness enabling long-range optical phonon dispersion[7] and self-healing properties,[8] strong electron–phonon coupling allowing long excited-state lifetimes and carrier mobility,[9] direct optical transitions contributing to high absorption coefficients ($\alpha \approx 2 \times 10^4$ cm^{-1}), long-lived excited states exceeding a microsecond and good tolerance of electronic defects.[10–14] Material processing is also peculiar if we consider that from a simple solution process associated with a mild and rapid post-annealing treatment, you can obtain a well-structured polycrystalline film with physical properties analogous to single crystals. However, perovskites still face significant problems, particularly environmentally with soluble lead and the harmful solvents used for processing,[15] and technically with their high sensitivity to almost all relevant external stressors, such as temperature,[16,17] humidity,[18–21] light[22,23] and electrical bias.[24] These two downsides are the main barriers to capitalizing research efforts towards industrialization.[25,26] With regards to stability, the problem has multifactorial causes. The degradation pathways are composition dependent,[27] defect dependent,[28,29] and subject to perovskite dimensionality[30] while the interface with the extraction layers (H/ETLs) also affects the degradation pathways and kinetics.[28,31,32]

For the last few years, formamidinium lead iodide (α-$FAPbI_3$) has been the state-of-the art composition owing to its low bandgap value of 1.49 eV[5,33] and greater thermal stability compared to its methylammonium counterpart.[34,35] However, the photo-active cubic structure is not the thermodynamically stable polymorph owing to its tolerance factor being a little greater than 1,[36] straddling the hexagonal yellow phase.[37] The community has come up with a wealth of propositions to stabilise the cubic polymorph through additive engineering,[32,38,39] structural modification using low-dimensional perovskite,[30,40] or by controlling the deposition process.[29] Understanding the degradation pathways from seeds to their longer-range propagation is essential for a comprehensive understanding of the reactivity of the material under stress. To this end, an *in situ* approach under external stress conditions is most relevant, given that perovskites can additionally self-heal when the external stress is stopped.[8] Only a very few reports involve *in situ* techniques for monitoring degradation, focusing on X-ray diffraction, transmission electron microscopy (TEM), or visible/infrared spectroscopy under different conditions (humidity, temperature, light, applied voltage).[21,23,41–46] Electron paramagnetic resonance spectroscopy (EPR) has also been used in the field of solar cells to probe the accumulation of photogenerated radicals under light.[47–49] Radical accumulation is correlated with a loss of cell performance; thus it is suspected to be one origin of the degradation mechanisms.[48] Temperature is another stringent stressor due to the structural softness of the hybrid perovskite, the content of organic moieties and the large propensity for vacancy formation.[50] When combined with light, the degradation kinetics could even be accelerated, although these studies were carried out under anoxic conditions.[51,52] In previous work, structural information on the thermal and

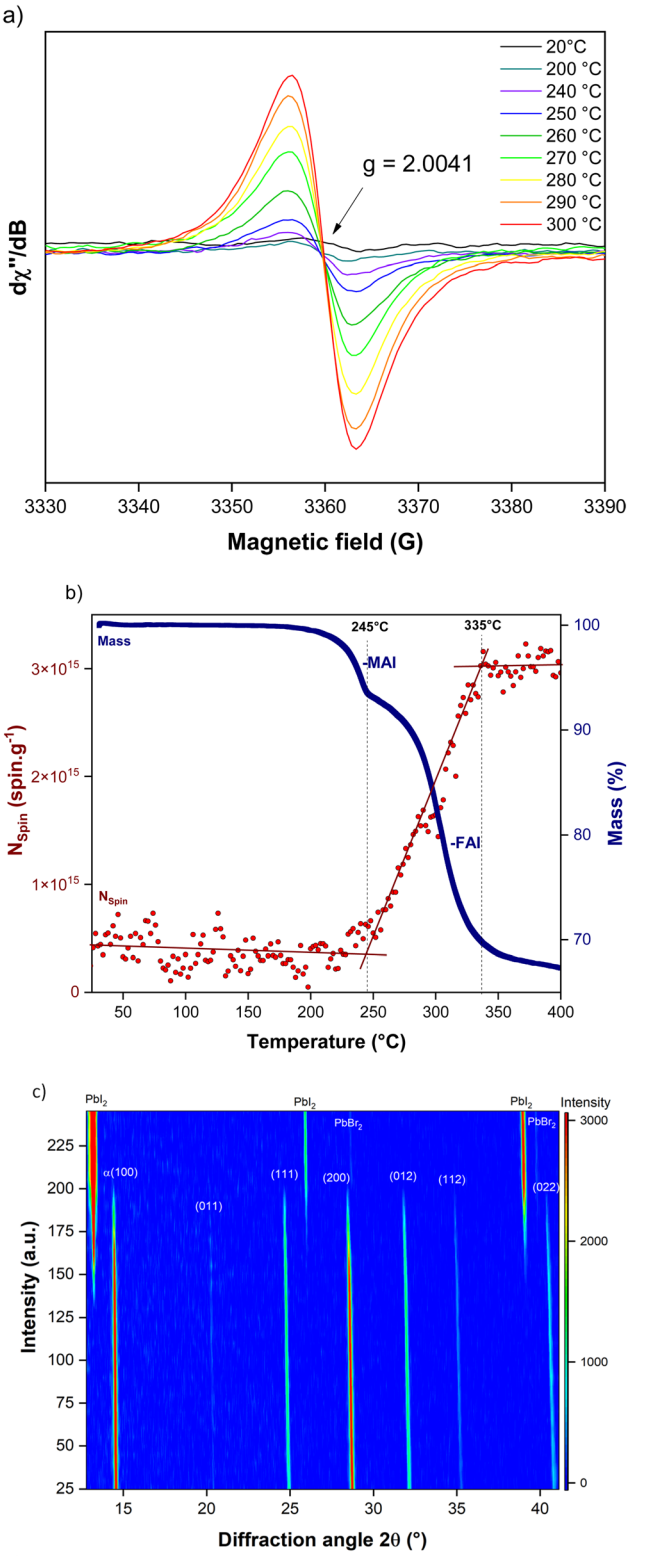

Fig. 1 (a) *In situ* evolution of the electron paramagnetic resonance spectrum of (FA-MA)PbI_3 in the dark upon heating between 20 °C and 300 °C. (b) Comparative plot showing the evolution of the spin density in the perovskite film (red) and mass evolution of the perovskite measured by TGA-MS analysis (blue) as a function of temperature. (c) 2D contour plot representation of the *in situ* X-ray diffraction study as a function of temperature between 25 °C and 245 °C for (FA-MA)PbI_3 in the dark.

Open Access Article. Published on 21 January 2025. Downloaded on 1/22/2026 1:24:09 AM.
This article is licensed under a Creative Commons Attribution-NonCommercial 3.0 Unported Licence.

photodecomposition of $(FA_{0.73}MA_{0.27})Pb(I_{0.945}Br_{0.055})_3$ under an ambient atmosphere was reported based on *in situ* X-ray diffraction.[53] We highlighted that this perovskite degradation is substantially accelerated when temperature is combined with light and when it is interfaced with the extraction layers. We also revealed the existence of a temperature gap region forming exclusively under illumination, in which an intermediate disordered phase is involved between perovskite decomposition and PbI_2 formation. In this work, we captured complementary information by linking structural to electronic information on the seed origin of this photo-induced and thermal degradation by means of *in situ* electron paramagnetic resonance (EPR) spectroscopy. This technique offers high sensitivity to the formation of free carriers while revealing very valuable insights into electronic interactions on materials and interfaced materials.[47,49,54,55]

Results and discussion

The procedure for the preparation of different samples is described in the experimental section. All the films have a homogeneous and a mirror-like aspect. The incorporation of MABr into α-$FAPbI_3$ allows the crystallisation of a pure α-phase (Fig. S1a†). The refined lattice cell parameter (a = 6.3315 Å) is slightly reduced from that reported in the literature for pure α-$FAPbI_3$ (a = 6.35 Å), suggesting that an amount of MABr is incorporated into the final film.[56–58] Indeed, by considering Vegard's law, *i.e.* linear evolution of the lattice cell parameter depending on the amount of bromide in the film (Fig. S1b†), the final amount of Br^- incorporated in the film is around 5 mol%.[57,59] The bandgap value, calculated based on absorption spectroscopic data, shows a bandgap of 1.55 eV, compared to 1.49 eV for pure α-$FAPbI_3$ (Fig. S1c†).[60] The final perovskite composition was further confirmed by EDX analysis where an atomic ratio of Br/I of 0.05 was consistently found (Fig. S1d†).

Fig. 1a shows the *in situ* evolution of the EPR signal of the perovskite in darkness between 20 °C and 400 °C. The g-factor is equal to 2.0041 regardless of temperature. This value corresponds to an electron stabilized in the π orbital of carbon.[61] Both the shape and intensity of this paramagnetic signal are similar from room temperature up to 245 °C, indicating no change in the chemical environment and no drastic evolution of the spin concentration in the perovskite film, which was determined to be $N_{spin} = 5 \times 10^{14}$ spin per g. The very slight decrease in spin density stems from the higher recombination of carriers with temperature. The value of 5×10^{14} spin per g is in a similar range to that of the spin concentration reported for $MAPbI_3$ film under similar conditions (*ca.* 10^{14} spin per g).[48,62] Interestingly, thermogravimetric analysis (TGA) performed under air combined with mass spectrometry shows that the perovskite film is not thermally stable in this temperature region.[17] A first mass loss of 6.9% is observed at an onset temperature of 163 °C up to *ca.* 245 °C (Fig. 1b). This corresponds to the release of either methylammonium iodide or methylamine and HI from the perovskite structure. This allows us, along with structural refinement of the lattice cell parameters, to determine the exact stoichiometry of our perovskite film, which is $FA_{0.73}MA_{0.27}Pb(I_{0.95}Br_{0.05})_3$ and will be referred to as "(FA-MA)PbI_3" in the following discussion. It is interesting to note that almost all the methylammonium used during film preparation is successfully incorporated into the perovskite structure in contrast to the bromide. The excess of formamidinium and bromide is washed away during anti-solvent dripping.

In this temperature range, the perovskite structure degrades into crystalline PbI_2, crystalline $PbBr_2$ and a remaining X-ray-amorphous content, including formamidinium, lead and

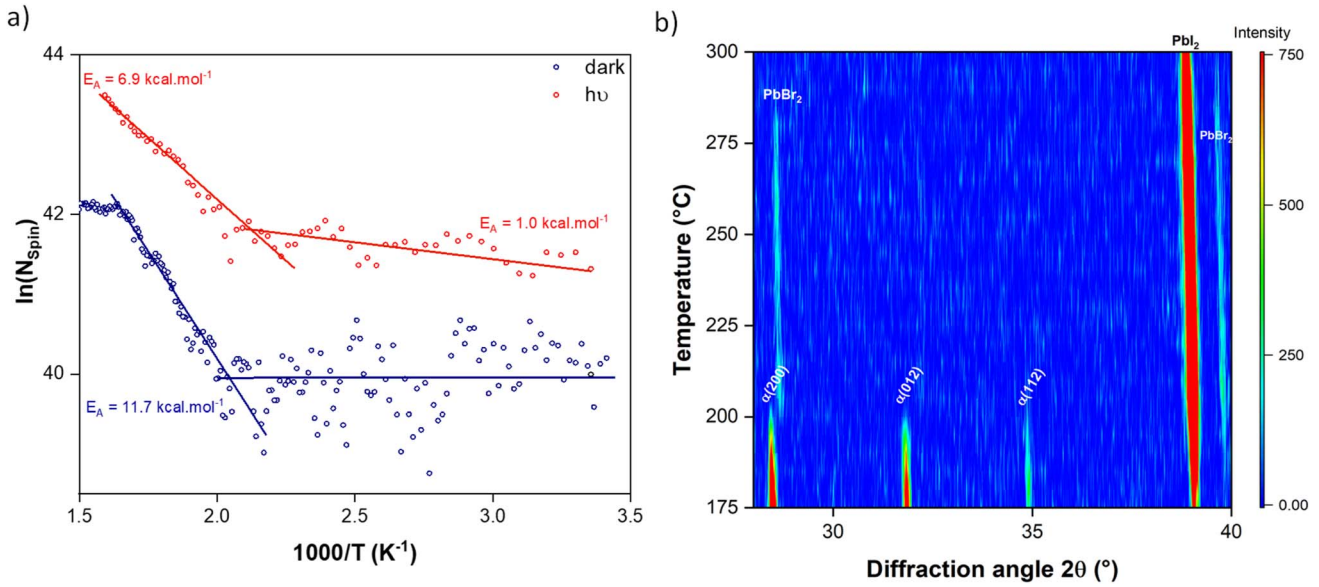

Fig. 2 (a) Arrhenius plot of spin concentration depending on temperature for the perovskite in the dark (blue) and under illumination (red) with the corresponding activation energies E_A. (b) 2D contour plot representation of *in situ* X-ray diffraction at temperatures between 175 °C and 300 °C for (FA-MA)PbI_3 film.

 © 2025 The Author(s). Published by the Royal Society of Chemistry

Open Access Article. Published on 21 January 2025. Downloaded on 1/22/2026 1:24:09 AM.
This article is licensed under a Creative Commons Attribution-NonCommercial 3.0 Unported Licence.

halide (Fig. 1c).[53] Consequently, we conclude that the first step of the thermal degradation of perovskite is not a radical-type process and is triggered by the high volatility of the methylammonium group.

By contrast, the EPR signal increases proportionally with temperature between 245 °C and 335 °C accordingly to an Arrhenius activation law (Fig. 2a). The radical concentration in the film reaches 3×10^{15} spin per g with a rate constant of $(2.7 \pm 0.1) \times 10^{13}$ spin per g per K. For higher temperatures, the number of radicals present in the film is stabilizing. This result is again well correlated with the TGA analysis. Indeed, above 245 °C, the rise in radicals relates to the second weight loss of 25.8% corresponding to the formamidinium iodide (FAI) located in the remaining amorphous content in the film, as supported by the *in situ* X-ray diffraction (Fig. 2b).[53] Thus, in contrast to the first weight loss, this degradation step has a clear radical origin, where the radicals are located in the carbon of the formamidinium cation, leading due to fragments of formamidinium cation, as deduced by mass spectrometry (Fig. S2†). The activation energy for this degradation reaction is 11.7 kcal mol^{-1} (Fig. S3†). For temperatures greater than 335 °C, the radicals formed are trapped in the remaining film. The latter is based on crystalline lead iodide and lead bromide and probably other amorphous content, without any organic groups remaining, as deduced from the final mass obtained from TGA analysis and correlated with the *in situ* X-ray diffraction (Fig. 2b).

The effect of temperature and illumination as combined stressors has been assessed. The resulting behaviour shows a stark difference upon light excitation, although the EPR signal of the perovskite film under illumination remains with a *g*-factor of 2.0040 corresponding to an electron stabilized in the π orbital of carbon (Fig. 3a). At room temperature, the spin density is three times higher under illumination (1.4×10^{15} spin per g) (Fig. 3b). This could be due to the accumulation of long-lived (>10 μs) free carriers in the perovskite film under illumination.[47–49] This concentration increases rapidly within the first minutes of illumination and reaches a steady-state value after 12 hours (Fig. S3†). Between room temperature and 220 °C, a slight increase in concentration is noticed, as one would expect due to the thermal activation of free carriers in semi-conductors. The Arrhenius thermal activation dependency is observed with an activation energy of 1 kcal mol^{-1} (Fig. 2a). This value refers to the energy barrier for the generation of free carriers and exciton dissociation induced by the temperature and the applied B^0 magnetic field (0.33 T) from EPR. Given that the same experiment in darkness shows that temperature makes no contribution, we can conclude that the exciton binding energy of (FA-MA)PbI_3 is 1 kcal mol^{-1}, corresponding to 43 meV for the cubic phase. This value is higher than the *ca.* 14 meV reported from the magneto-absorption technique by Nicholas *et al.* for $FAPbI_3$ at 2 K (orthorhombic unit cell)[63,64] and falls in a comparable range to earlier studies also performed at 4 K for $MAPbI_3$ (37–45 meV).[65,66] These results seem to confirm that the tetragonal-to-cubic phase transition is responsible for an increase in the excitonic binding energy, as previously discussed in the literature by Even *et al.* and Yamada *et al.*[67,68] The

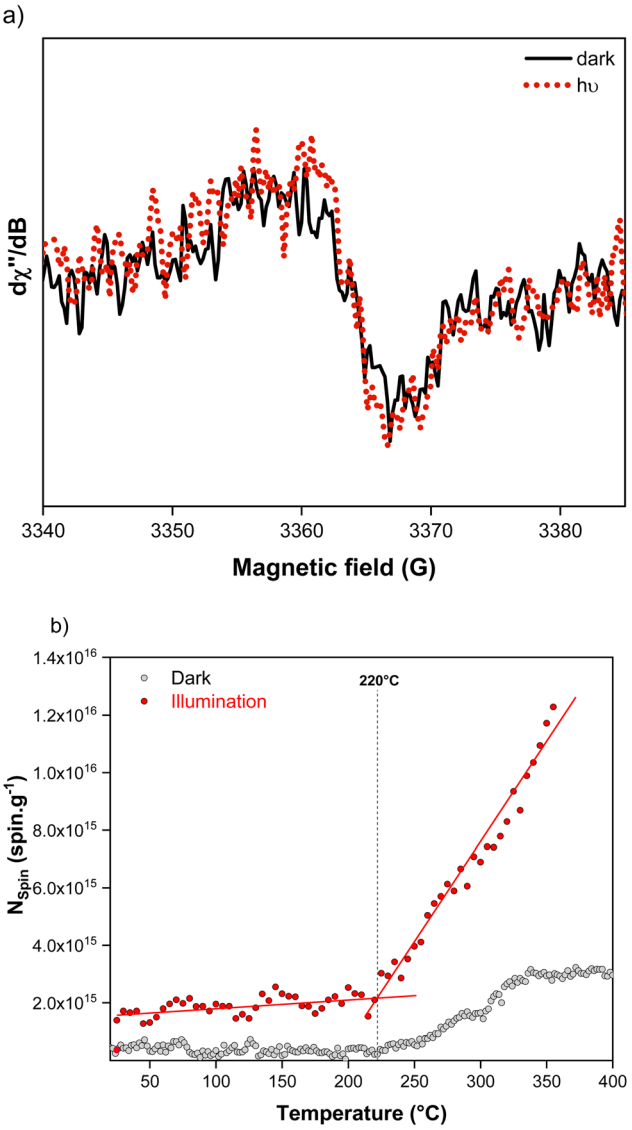

Fig. 3 (a) Comparison of EPR spectra of (FA-MA)PbI_3 in the dark (black line) and under illumination (red dashes) at 25 °C. (b) Comparison of the evolution of the spin density of (FA-MA)PbI_3 as a function of temperature in the dark (black) and under illumination (red). For illumination measurements, the lamp was turned on *ca.* 1 minute before starting the EPR acquisition.

quantity of radicals increases proportionally for temperatures above 220 °C and up to 350 °C. The rate constant of radical formation is $(6.8 \pm 0.24) \times 10^{13}$ spin per g per K, a value 2.5 times greater than that under darkness. These results confirm that the onset of radical formation takes place at a lower temperature than in darkness, by *ca.* 25 °C. This trend with free carrier generation can be linked with previous results based on *in situ* X-ray diffraction, in which we found that the onset of structural degradation of the perovskite under illumination took place at a temperature 35 °C lower than in darkness.[53] Nevertheless, it is also important to highlight that such threshold temperatures for the formation of new radicals are significantly higher than (i) the starting temperature of perovskite decomposition (*ca.* 110 °C), or (ii) the formation of PbI_2 as

Open Access Article. Published on 21 January 2025. Downloaded on 1/22/2026 1:24:09 AM.
This article is licensed under a Creative Commons Attribution-NonCommercial 3.0 Unported Licence.

a byproduct of degradation (*ca.* 125 °C).[53] The temperature of 220 °C correlates very well with the maximum content of PbI_2 in the film before its light-driven decomposition through radicals, or chemical reaction with the amorphous remainder.[23,69] Indeed, the increase in carbon-centred radicals in the material between 220 °C and 350 °C is more important than in the dark, suggesting that light favours their formation and therefore their reaction with PbI_2. The apparent activation energy for this photodecomposition reaction of PbI_2 is 6.9 kcal mol^{-1}.

In most of the reported literature on degradation mechanisms, little is said about the effect of the perovskite interfacing with the extraction layer, whereas it has a clear role in the instability of the perovskite layer, as it has been highlighted in previous work including that by our group.[20,53] We performed similar investigations with perovskite interfaced with doped spiro-OMeTAD, namely [2,2′,7,7′-tetrakis(*N*,*N*-di-*p*-methoxyphenyl-amine)-9,9′-spirobifluorene], as a hole transport layer (HTL) (Fig. 4). The *g*-value is 2.0048, whether in the dark or under illumination. This corresponds to the strong paramagnetic signal of the oxidized spiro-OMeTAD$^{+\bullet}$ radical cation, which herein hides the perovskite signal.[62] This *g*-value is slightly higher than the value reported in the literature for spiro-

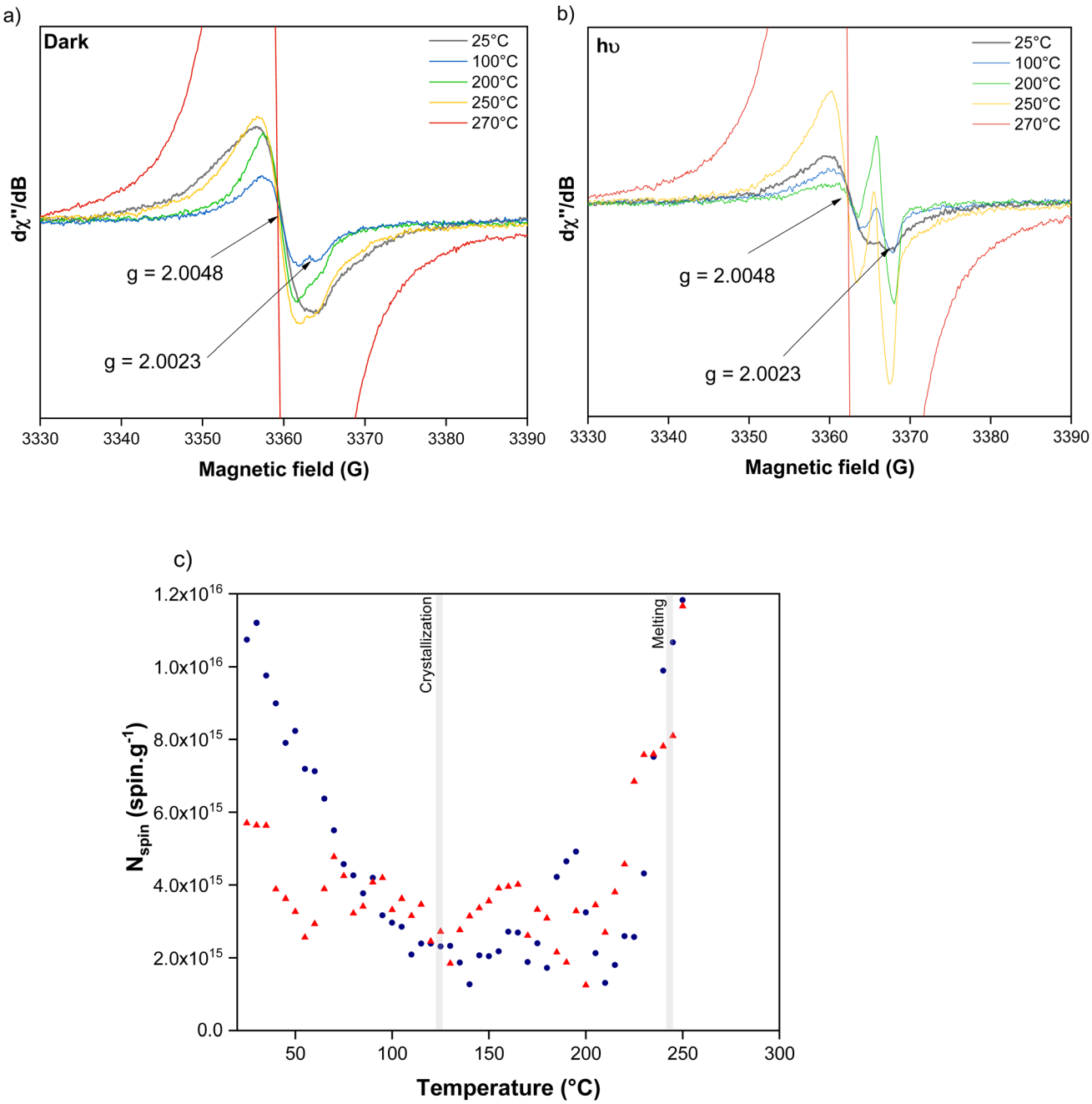

Fig. 4 Electron paramagnetic resonance spectroscopy on (FA-MA)PbI_3/spiro-OMeTAD as a function of temperature between 20 °C and 300 °C: (a) in the dark, (b) under illumination, (c) comparison of the evolution of spin concentration as a function of temperature in the dark (blue) and under illumination (red). For illumination measurements, the lamp was turned on *ca.* 1 minute before starting the EPR acquisition.

 © 2025 The Author(s). Published by the Royal Society of Chemistry

Open Access Article. Published on 21 January 2025. Downloaded on 1/22/2026 1:24:09 AM.
This article is licensed under a Creative Commons Attribution-NonCommercial 3.0 Unported Licence.

OMeTAD doped with LiTFSI (*ca.* $g = 2.0030$).[48,70,71] This suggests that the free electron in the spiro-OMeTAD$^{+\bullet}$ radical cation interacts strongly with the other components of the HTL blend, in particular $Co(bpy)_3^{3+}$ and *tert*-butylpyridine.

When the temperature is increasing, the *g*-value is not affected, whereas both the intensity and the shape of the first derivative absorption signal are drastically modified (Fig. 4a and b). The signal decreases in intensity and a shoulder appears due to a new paramagnetic contribution, with a *g*-value of 2.0023 corresponding to the free electron value (g_e). Note that under illumination, the new signal appearing is more intense than in the dark and continues to grow with temperature (Fig. S4†). Fig. 4c depicts the evolution of spin concentration. In the dark, the latter decreases by almost one order of magnitude, from 10^{16} spin per g down to 2×10^{15} spin per g at *ca.* 140 °C. This result underlines that temperature induces a de-doping mechanism in spiro-OMeTAD either through a redox reaction with air or by disrupting the intricate molecular interactions between the HTM and the additives.[72] This trend is also observed when the spiro-OMeTAD is not in contact with the perovskite, ruling out the potential effect of the latter in this deactivation path (Fig. S5†). In the temperature range between 140 °C and 230 °C, the spin concentration is rather constant (2×10^{15} spin per g), before increasing again beyond 10^{16} spin per g (Fig. 4c). Differential scanning calorimetry experiments were carried out to collect more information about the thermal behaviour of spiro-OMeTAD (Fig. S6†). The exothermic heat exchange at 128 °C is ascribed to crystallization of the disordered doped spiro-OMeTAD. The endothermic peak at 244 °C corresponds to the melting point. Interestingly, the doping agents substantially lower the crystallization temperature by *ca.* 40 °C (the crystallization temperature of undoped spiro-OMeTAD is 165 °C). This results from two aspects. First, there are strong molecular interactions between the HTM and the dopants. Secondly, it stems from slight modification of the crystal structure, which influences the mesoscale packing of spiro-OMeTAD molecules.[73] In relation to this, the energy released during crystallization is also noticeably affected, −12.98 J g^{-1} when doped compared to −5.47 J g^{-1} for the undoped counterpart. Consistently, the evolution of the EPR signal correlates with this calorimetric study. After crystallization, the de-doping reaction stops and the free carriers generated from the thermal activation compensate with the rate of recombination. The plateau observed for N_{Spin} in this temperature range is not present when the spiro-OMeTAD is not in contact with the perovskite and in darkness (Fig. S5†), *i.e.* N_{Spin} keeps decreasing until melting in contrast to the case under illumination. It is worth mentioning that this plateau is also visible when the perovskite is in contact with the HTL, both in the dark and under illumination (Fig. 4c). This is likely to be the result of the first steps of perovskite degradation, taking place in this temperature range when it is interfaced with the HTL.[53] To account for these observations, we can raise the hypothesis that the byproducts from perovskite degradation, *i.e.* methylammonium and/or iodide/iodine, interact with the spiro-OMeTAD molecules and eventually also modify the interactions between the spiro-OMeTAD and the additives (*e.g.* replacing $TFSI^-$ by I^- and/or lithium by methylammonium).[72]

By contrast, light excitation of undoped spiro-OMeTAD induces a self-doping mechanism. This is confirmed by the continuous increase in spin density with time at room temperature, in agreement with previous studies based on UV-visible absorption spectroscopy and conductivity measurements (Fig. S7†).[74,75]

For spiro-OMeTAD in contact with (FA-MA)PbI_3 under illumination (Fig. 4b and c), the evolution of signal intensity is similar to that in darkness, *i.e.* a decrease with temperature until crystallization. By comparing the concentrations in darkness and under illumination, one can see that the concentration at room temperature is lower under illumination, 6×10^{15} spin per g and 10^{16} spin per g, respectively. This result is the outcome of the photogenerated carriers within the perovskite recombining at the interface with the HTL, making them undetectable by EPR spectroscopy.[76,77] In the dark, the spin concentration decreases until around 130 °C, but at a slower rate, reaching a comparable concentration of 2×10^{15} spin per g before increasing to 1×10^{16} spin per g at a rate of $(1.9 \pm 0.2) \times 10^{14}$ spin per g per K until melting (*ca.* 250 °C). This rate is relatively similar to that in the dark: $(2.9 \pm 0.3) \times 10^{14}$ spin per g per K.

Conclusions

We have herein reported the thermal and photodegradation behaviour of $(FA_{0.73}MA_{0.27})Pb(I_{0.945}Br_{0.055})_3$ alone and when interfaced with spiro-OMeTAD by using *in situ* EPR spectroscopy. The results from probing free carriers are well corroborated with the structural evolution studied by *in situ* X-ray diffraction, and its thermal stability by thermogravimetric and calorimetric analysis. In this work, we have demonstrated that perovskite decomposition under heating proceeds in two steps. The first involves a non-radical-based degradation inducing methylammonium and iodide release. This is in contrast with the second step that involves the remaining formamidinium, iodide and bromide in the already decomposed perovskite, in which this further decomposition is mediated by radicals localized in the carbon of the formamidinium leading to the release of formamidinium fragments. The thermal behaviour of spiro-OMeTAD has also been clarified. More particularly, EPR spectroscopy confirms the self-doping reaction of pristine spiro-OMeTAD under continuous illumination. However, when chemically doped, our results underline the harmful effect of temperature, which translates into a de-doping reaction of the oxidized spiro-OMeTAD$^{+\bullet}$ radical cation. This mechanism is particularly deleterious for full device operation under ageing under temperature stress. Finally, combining temperature, magnetic field and illumination, we determined that the exciton binding energy at room temperature of cubic (FA-MA)PbI_3 is 43 meV.

Data availability

The data supporting this article have been included as part of the ESI.† All data related to *in situ* investigations will be available upon request from the authors (>1 Gb).

Open Access Article. Published on 21 January 2025. Downloaded on 1/22/2026 1:24:09 AM.
This article is licensed under a Creative Commons Attribution-NonCommercial 3.0 Unported Licence.

Conflicts of interest

The authors declare no conflict of interest.

Acknowledgements

F. S. acknowledges EU financial support through the European Research Council program (ERC-2023-AdG) "GEMINI" project, under grant agreement number 101141284. We thank the INFRANALYTICS FR2054 EPR platform at the University of Lille for assessing EPR facilities. We thank Dr Jean-Noël Chotard, Associate Prof. at LRCS, for insightful discussions about the XRD data. F. S. and J. R. acknowledges financial support of the French Ministry of Research for her Ph-D grant.

References

1 M. A. Green, E. D. Dunlop, M. Yoshita, N. Kopidakis, K. Bothe, G. Siefer and X. Hao, Solar Cell Efficiency Tables (Version 62), *Prog. Photovoltaics*, 2023, **31**(7), 651–663, DOI: 10.1002/pip.3726.

2 NREL, P. research, Best Research Cell Efficiency Chart, https://www.nrel.gov/pv/cell-efficiency.html, accessed 2024-01-11.

3 Q. Lin, D. J. Kubicki, M. Omrani, F. Alam and M. Abdi-Jalebi, The Race between Complicated Multiple Cation/Anion Compositions and Stabilization of $FAPbI_3$ for Halide Perovskite Solar Cells, *J. Mater. Chem. C*, 2023, **11**(7), 2449–2468, DOI: 10.1039/D2TC04529J.

4 W. Ke and M. G. Kanatzidis, Prospects for Low-Toxicity Lead-Free Perovskite Solar Cells, *Nat. Commun.*, 2019, **10**(1), 965, DOI: 10.1038/s41467-019-08918-3.

5 J. Jeong, M. Kim, J. Seo, H. Lu, P. Ahlawat, A. Mishra, Y. Yang, M. A. Hope, F. T. Eickemeyer, M. Kim, Y. J. Yoon, I. W. Choi, B. P. Darwich, S. J. Choi, Y. Jo, J. H. Lee, B. Walker, S. M. Zakeeruddin, L. Emsley, U. Rothlisberger, A. Hagfeldt, D. S. Kim, M. Grätzel and J. Y. Kim, Pseudo-Halide Anion Engineering for α-$FAPbI_3$ Perovskite Solar Cells, *Nature*, 2021, **592**(7854), 381–385, DOI: 10.1038/s41586-021-03406-5.

6 S. Gholipour and M. Saliba, Bandgap Tuning and Compositional Exchange for Lead Halide Perovskite Materials, in *Characterization Techniques for Perovskite Solar Cell Materials*, Elsevier, 2020, pp. 1–22, DOI: 10.1016/B978-0-12-814727-6.00001-3.

7 J. Yang, X. Wen, H. Xia, R. Sheng, Q. Ma, J. Kim, P. Tapping, T. Harada, T. W. Kee, F. Huang, Y.-B. Cheng, M. Green, A. Ho-Baillie, S. Huang, S. Shrestha, R. Patterson and G. Conibeer, Acoustic-Optical Phonon Up-Conversion and Hot-Phonon Bottleneck in Lead-Halide Perovskites, *Nat. Commun.*, 2017, **8**(1), 14120, DOI: 10.1038/ncomms14120.

8 B. P. Finkenauer, Akriti, K. Ma and L. Dou, Degradation and Self-Healing in Perovskite Solar Cells, *ACS Appl. Mater. Interfaces*, 2022, **14**(21), 24073–24088, DOI: 10.1021/acsami.2c01925.

9 A. D. Wright, C. Verdi, R. L. Milot, G. E. Eperon, M. A. Pérez-Osorio, H. J. Snaith, F. Giustino, M. B. Johnston and L. M. Herz, Electron–Phonon Coupling in Hybrid Lead Halide Perovskites, *Nat. Commun.*, 2016, **7**(1), 11755, DOI: 10.1038/ncomms11755.

10 T. M. Brenner, D. A. Egger, A. M. Rappe, L. Kronik, G. Hodes and D. Cahen, Are Mobilities in Hybrid Organic–Inorganic Halide Perovskites Actually "High"?, *J. Phys. Chem. Lett.*, 2015, **6**(23), 4754–4757, DOI: 10.1021/acs.jpclett.5b02390.

11 V. D'Innocenzo, G. Grancini, M. J. P. Alcocer, A. R. S. Kandada, S. D. Stranks, M. M. Lee, G. Lanzani, H. J. Snaith and A. Petrozza, Excitons versus Free Charges in Organo-Lead Tri-Halide Perovskites, *Nat. Commun.*, 2014, **5**(1), 3586, DOI: 10.1038/ncomms4586.

12 T. M. Brenner, D. A. Egger, A. M. Rappe, L. Kronik, G. Hodes and D. Cahen, Low Trap-State Density and Long Carrier Diffusion in Organolead Trihalide Perovskite Single Crystals, *Science*, 2015, **347**(6221), 519–522.

13 M. B. Johnston and L. M. Herz, Hybrid Perovskites for Photovoltaics: Charge-Carrier Recombination, Diffusion, and Radiative Efficiencies, *Acc. Chem. Res.*, 2016, **49**(1), 146–154, DOI: 10.1021/acs.accounts.5b00411.

14 G. Xing, N. Mathews, S. Sun, S. Sien Lim, Y. Ming Lam, M. Graetzel, S. G. Mhaisalkar and T. Chien Sum, Long-Range Balanced Electron- and Hole-Transport Lengths in Organic-Inorganic $CH_3NH_3PbI_3$, *Science*, 2013, **342**, 344–347, DOI: 10.1126/science.1243167.

15 G. Ding, Y. Zheng, X. Xiao, H. Cheng, G. Zhang, Y. Shi and Y. Shao, Sustainable Development of Perovskite Solar Cells: Keeping a Balance between Toxicity and Efficiency, *J. Mater. Chem. A*, 2022, **10**(15), 8159–8171, DOI: 10.1039/D2TA00248E.

16 T. T. Ava, A. Al Mamun, S. Marsillac and G. Namkoong, A Review: Thermal Stability of Methylammonium Lead Halide Based Perovskite Solar Cells, *Appl. Sci.*, 2019, **9**(1), 188, DOI: 10.3390/app9010188.

17 L. Ma, D. Guo, M. Li, C. Wang, Z. Zhou, X. Zhao, F. Zhang, Z. Ao and Z. Nie, Temperature-Dependent Thermal Decomposition Pathway of Organic–Inorganic Halide Perovskite Materials, *Chem. Mater.*, 2019, **31**(20), 8515–8522, DOI: 10.1021/acs.chemmater.9b03190.

18 Z. Lin, Y. Zhang, M. Gao, J. A. Steele, S. Louisia, S. Yu, L. N. Quan, C.-K. Lin, D. T. Limmer and P. Yang, Kinetics of Moisture-Induced Phase Transformation in Inorganic Halide Perovskite, *Matter*, 2021, **4**(7), 2392–2402, DOI: 10.1016/j.matt.2021.04.023.

19 E. Akman, A. E. Shalan, F. Sadegh and S. Akin, Moisture-Resistant $FAPbI_3$ Perovskite Solar Cell with 22.25% Power Conversion Efficiency through Pentafluorobenzyl Phosphonic Acid Passivation, *ChemSusChem*, 2021, **14**(4), 1176–1183, DOI: 10.1002/cssc.202002707.

20 M. A. Akhavan Kazemi, P. Raval, K. Cherednichekno, J.-N. Chotard, A. Krishna, A. Demortiere, G. N. M. Reddy and F. Sauvage, Molecular-Level Insight into Correlation between Surface Defects and Stability of Methylammonium Lead Halide Perovskite under Controlled Humidity, *Small Methods*, 2021, **5**(2), 2000834, DOI: 10.1002/smtd.202000834.

 © 2025 The Author(s). Published by the Royal Society of Chemistry

Open Access Article. Published on 21 January 2025. Downloaded on 1/22/2026 1:24:09 AM.
This article is licensed under a Creative Commons Attribution-NonCommercial 3.0 Unported Licence.

21 M. A. A. Kazemi, N. Folastre, P. Raval, M. Sliwa, J. M. V. Nsanzimana, S. Golonu, A. Demortiere, J. Rousset, O. Lafon, L. Delevoye, G. N. M. Reddy and F. Sauvage, Moisture-Induced Non-Equilibrium Phase Segregation in Triple Cation Mixed Halide Perovskite Monitored by In Situ Characterization Techniques and Solid-State NMR, *Energy Environ. Mater.*, 2022, 1–10, DOI: 10.1002/eem2.12335.

22 N. A. Emelianov, V. V. Ozerova, I. S. Zhidkov, D. V. Korchagin, G. V. Shilov, A. L. Litvinov, E. Z. Kurmaev, L. A. Frolova, S. M. Aldoshin and P. A. Troshin, Nanoscale Visualization of Photodegradation Dynamics of $MAPbI_3$ Perovskite Films, *J. Phys. Chem. Lett.*, 2022, **13**(12), 2744–2749, DOI: 10.1021/acs.jpclett.2c00497.

23 A. F. Akbulatov, S. Yu. Luchkin, L. A. Frolova, N. N. Dremova, K. L. Gerasimov, I. S. Zhidkov, D. V. Anokhin, E. Z. Kurmaev, K. J. Stevenson and P. A. Troshin, Probing the Intrinsic Thermal and Photochemical Stability of Hybrid and Inorganic Lead Halide Perovskites, *J. Phys. Chem. Lett.*, 2017, **8**(6), 1211–1218, DOI: 10.1021/acs.jpclett.6b03026.

24 K. M. Anoop, M. Khenkin, F. Di Giacomo, Y. Galagan, S. Rahmany, L. Etgar, E. Katz and I. Visoly-Fisher, Bias-Dependent Stability of Perovskite Solar Cells Studied Using Natural and Concentrated Sunlight, *Sol. RRL*, 2020, **4**, 1900335.

25 D. Bryant, N. Aristidou, S. Pont, I. Sanchez-Molina, T. Chotchunangatchaval, S. Wheeler, J. R. Durrant and S. A. Haque, Light and Oxygen Induced Degradation Limits the Operational Stability of Methylammonium Lead Triiodide Perovskite Solar Cells, *Energy Environ. Sci.*, 2016, **9**(5), 1655–1660, DOI: 10.1039/C6EE00409A.

26 P. Tonui, S. O. Oseni, G. Sharma, Q. Yan and G. Tessema Mola, Perovskites Photovoltaic Solar Cells: An Overview of Current Status, *Renewable Sustainable Energy Rev.*, 2018, **91**, 1025–1044, DOI: 10.1016/j.rser.2018.04.069.

27 T. H. Chan, N. T. Taylor, S. Sundaram and S. P. Hepplestone, Phase Stability and Electronic Properties of Hybrid Organic–Inorganic Perovskite Solid Solution $(CH(NH_2)_2)_x(CH_3NH_3)_{1-x}Pb(BryI_{1-y})_3$ as a Function of Composition, *J. Phys. Chem. C*, 2022, **126**(32), 13640–13648, DOI: 10.1021/acs.jpcc.2c03555.

28 A. Krishna, M. A. Akhavan Kazemi, M. Sliwa, G. N. M. Reddy, L. Delevoye, O. Lafon, A. Felten, M. T. Do, S. Gottis and F. Sauvage, Defect Passivation via the Incorporation of Tetrapropylammonium Cation Leading to Stability Enhancement in Lead Halide Perovskite, *Adv. Funct. Mater.*, 2020, **30**(13), 1909737, DOI: 10.1002/adfm.201909737.

29 H. Lu, Y. Liu, P. Ahlawat, A. Mishra, W. R. Tress, F. T. Eickemeyer, Y. Yang, F. Fu, Z. Wang, C. E. Avalos, B. I. Carlsen, A. Agarwalla, X. Zhang, X. Li, Y. Zhan, S. M. Zakeeruddin, L. Emsley, U. Rothlisberger, L. Zheng, A. Hagfeldt and M. Grätzel, Vapor-Assisted Deposition of Highly Efficient, Stable Black-Phase $FAPbI_3$ Perovskite Solar Cells, *Science*, 2020, **370**(6512), eabb8985, DOI: 10.1126/science.abb8985.

30 R. Hu, Y. Zhang, S. Paek, X.-X. Gao, X. Li and M. K. Nazeeruddin, Enhanced Stability of α-Phase $FAPbI_3$ Perovskite Solar Cells by Insertion of 2D $(PEA)_2PbI_4$ Nanosheets, *J. Mater. Chem. A*, 2020, **8**(16), 8058–8064, DOI: 10.1039/C9TA14207J.

31 F. Gao, Y. Zhao, X. Zhang and J. You, Recent Progresses on Defect Passivation toward Efficient Perovskite Solar Cells, *Adv. Energy Mater.*, 2020, **10**(13), 1902650, DOI: 10.1002/aenm.201902650.

32 H. Zhu, Y. Liu, F. T. Eickemeyer, L. Pan, D. Ren, M. A. Ruiz-Preciado, B. Carlsen, B. Yang, X. Dong, Z. Wang, H. Liu, S. Wang, S. M. Zakeeruddin, A. Hagfeldt, M. I. Dar, X. Li and M. Grätzel, Tailored Amphiphilic Molecular Mitigators for Stable Perovskite Solar Cells with 23.5% Efficiency, *Adv. Mater.*, 2020, **32**(12), 1907757, DOI: 10.1002/adma.201907757.

33 Y. Zhang, T. Kong, H. Xie, J. Song, Y. Li, Y. Ai, Y. Han and D. Bi, Molecularly Tailored SnO_2/Perovskite Interface Enabling Efficient and Stable $FAPbI_3$ Solar Cells, *ACS Energy Lett.*, 2022, **7**(3), 929–938, DOI: 10.1021/acsenergylett.1c02545.

34 F. Valipour, E. Yazdi, N. Torabi, B. F. Mirjalili and A. Behjat, Improvement of the Stability of Perovskite Solar Cells in Terms of Humidity/Heat via Compositional Engineering, *J. Phys. D: Appl. Phys.*, 2020, **53**(28), 285501, DOI: 10.1088/1361-6463/ab8511.

35 J. Kim, N. Park, J. S. Yun, S. Huang, M. A. Green and A. W. Y. Ho-Baillie, An Effective Method of Predicting Perovskite Solar Cell Lifetime–Case Study on Planar $CH_3NH_3PbI_3$ and $HC(NH_2)_2PbI_3$ Perovskite Solar Cells and Hole Transfer Materials of Spiro-OMeTAD and PTAA, *Sol. Energy Mater. Sol. Cells*, 2017, **162**, 41–46, DOI: 10.1016/j.solmat.2016.12.043.

36 Z. Li, M. Yang, J.-S. Park, S.-H. Wei, J. J. Berry and K. Zhu, Stabilizing Perovskite Structures by Tuning Tolerance Factor: Formation of Formamidinium and Cesium Lead Iodide Solid-State Alloys, *Chem. Mater.*, 2016, **28**(1), 284–292, DOI: 10.1021/acs.chemmater.5b04107.

37 S. Masi, A. F. Gualdrón-Reyes and I. Mora-Seró, Stabilization of Black Perovskite Phase in $FAPbI_3$ and $CsPbI_3$, *ACS Energy Lett.*, 2020, **5**(6), 1974–1985, DOI: 10.1021/acsenergylett.0c00801.

38 F. Ye, J. Ma, C. Chen, H. Wang, Y. Xu, S. Zhang, T. Wang, C. Tao and G. Fang, Roles of MACl in Sequentially Deposited Bromine-Free Perovskite Absorbers for Efficient Solar Cells, *Adv. Mater.*, 2021, **33**(3), 2007126, DOI: 10.1002/adma.202007126.

39 X. Zheng, C. Wu, S. K. Jha, Z. Li, K. Zhu and S. Priya, Improved Phase Stability of Formamidinium Lead Triiodide Perovskite by Strain Relaxation, *ACS Energy Lett.*, 2016, **1**(5), 1014–1020, DOI: 10.1021/acsenergylett.6b00457.

40 S. Masi, C. Echeverría-Arrondo, K. M. M. Salim, T. T. Ngo, P. F. Mendez, E. López-Fraguas, D. F. Macias-Pinilla, J. Planelles, J. I. Climente and I. Mora-Seró, Chemi-Structural Stabilization of Formamidinium Lead Iodide Perovskite by Using Embedded Quantum Dots, *ACS Energy*

Open Access Article. Published on 21 January 2025. Downloaded on 1/22/2026 1:24:09 AM.
This article is licensed under a Creative Commons Attribution-NonCommercial 3.0 Unported Licence.

Lett., 2020, **5**(2), 418–427, DOI: 10.1021/acsenergylett.9b02450.

41 G. Divitini, S. Cacovich, F. Matteocci, L. Cinà, A. Di Carlo and C. Ducati, In Situ Observation of Heat-Induced Degradation of Perovskite Solar Cells, *Nat. Energy*, 2016, **1**(2), 15012, DOI: 10.1038/nenergy.2015.12.

42 J. Yang, B. D. Siempelkamp, D. Liu and T. L. Kelly, Investigation of $CH_3NH_3PbI_3$ Degradation Rates and Mechanisms in Controlled Humidity Environments Using In Situ Techniques, *ACS Nano*, 2015, **9**(2), 1955–1963, DOI: 10.1021/nn506864k.

43 F. U. Kosasih and C. Ducati, Characterising Degradation of Perovskite Solar Cells through In-Situ and Operando Electron Microscopy, *Nano Energy*, 2018, **47**, 243–256, DOI: 10.1016/j.nanoen.2018.02.055.

44 B.-A. Chen, J.-T. Lin, N.-T. Suen, C.-W. Tsao, T.-C. Chu, Y.-Y. Hsu, T.-S. Chan, Y.-T. Chan, J.-S. Yang, C.-W. Chiu and H. M. Chen, In Situ Identification of Photo- and Moisture-Dependent Phase Evolution of Perovskite Solar Cells, *ACS Energy Lett.*, 2017, **2**(2), 342–348, DOI: 10.1021/acsenergylett.6b00698.

45 F. Baumann, S. R. Raga and M. Lira-Cantú, *Monitoring the Stability and Degradation Mechanisms of Perovskite Solar Cells by In Situ and Operando Characterization*, 2023.

46 R. Szostak, A. De Souza Gonçalves, J. N. De Freitas, P. E. Marchezi, F. L. De Araújo, H. C. N. Tolentino, M. F. Toney, F. Das Chagas Marques and A. F. Nogueira, *In Situ* and *Operando* Characterizations of Metal Halide Perovskite and Solar Cells: Insights from Lab-Sized Devices to Upscaling Processes, *Chem. Rev.*, 2023, **123**(6), 3160–3236, DOI: 10.1021/acs.chemrev.2c00382.

47 T. Nagamori and K. Marumoto, Direct Observation of Hole Accumulation in Polymer Solar Cells during Device Operation Using Light-Induced Electron Spin Resonance, *Adv. Mater.*, 2013, **25**(16), 2362–2367, DOI: 10.1002/adma.201204015.

48 M. Namatame, M. Yabusaki, T. Watanabe, Y. Ogomi, S. Hayase and K. Marumoto, Direct Observation of Dramatically Enhanced Hole Formation in a Perovskite-Solar-Cell Material Spiro-OMeTAD by Li-TFSI Doping, *Appl. Phys. Lett.*, 2017, **110**(12), 123904, DOI: 10.1063/1.4977789.

49 D. Son, T. Kuwabara, K. Takahashi and K. Marumoto, Direct Observation of UV-Induced Charge Accumulation in Inverted-Type Polymer Solar Cells with a TiO_x Layer: Microscopic Elucidation of the Light-Soaking Phenomenon, *Appl. Phys. Lett.*, 2016, **109**(13), 133301, DOI: 10.1063/1.4963285.

50 Y. W. Woo, Y.-K. Jung, G. Y. Kim, S. Kim and A. Walsh, Factors Influencing Halide Vacancy Transport in Perovskite Solar Cells, *Discover Mater.*, 2022, **2**(1), 8, DOI: 10.1007/s43939-022-00029-z.

51 A. F. Akbulatov, M. I. Ustinova, G. V. Shilov, N. N. Dremova, I. S. Zhidkov, E. Z. Kurmaev, L. A. Frolova, A. F. Shestakov, S. M. Aldoshin and P. A. Troshin, Temperature Dynamics of $MAPbI_3$ and PbI_2 Photolysis: Revealing the Interplay between Light and Heat, Two Enemies of Perovskite Photovoltaics, *J. Phys. Chem. Lett.*, 2021, **12**(18), 4362–4367, DOI: 10.1021/acs.jpclett.1c00883.

52 A. F. Akbulatov, L. A. Frolova, N. N. Dremova, I. Zhidkov, V. M. Martynenko, S. A. Tsarev, S. Yu. Luchkin, E. Z. Kurmaev, S. M. Aldoshin, K. J. Stevenson and P. A. Troshin, Light or Heat: What Is Killing Lead Halide Perovskites under Solar Cell Operation Conditions?, *J. Phys. Chem. Lett.*, 2020, **11**(1), 333–339, DOI: 10.1021/acs.jpclett.9b03308.

53 J. Ruellou, M. Courty and F. Sauvage, Thermal and Photo-Degradation Study of -$FAPbI_3$-Based Perovskite Using In Situ X-Ray, *Adv. Funct. Mater.*, 2023, **2300811**, 1–10.

54 K. Marumoto, T. Fujimori, M. Ito and T. Mori, Charge Formation in Pentacene Layers during Solar-Cell Fabrication: Direct Observation by Electron Spin Resonance, *Adv. Energy Mater.*, 2012, **2**, 591–597, DOI: 10.1002/aenm.201100774.

55 K. Marumoto, S. Kuroda, T. Takenobu and Y. Iwasa, Spatial Extent of Wave Functions of Gate-Induced Hole Carriers in Pentacene Field-Effect Devices as Investigated by Electron Spin Resonance, *Phys. Rev. Lett.*, 2006, **97**(25), 256603, DOI: 10.1103/PhysRevLett.97.256603.

56 T. Du, T. J. Macdonald, R. X. Yang, M. Li, Z. Jiang, L. Mohan, W. Xu, Z. Su, X. Gao, R. Whiteley, C.-T. Lin, G. Min, S. A. Haque, J. R. Durrant, K. A. Persson, M. A. McLachlan and J. Briscoe, Additive-Free, Low-Temperature Crystallization of Stable α-$FAPbI_3$ Perovskite, *Adv. Mater.*, 2022, **34**(9), 2107850, DOI: 10.1002/adma.202107850.

57 M. T. Weller, Cubic Perovskite Structure of Black Formamidinium Lead Iodide, α-$[HC(NH_2)_2]PbI_3$, at 298 K, *J. Phys. Chem. Lett.*, 2015, (6), 3209–3212.

58 Y. Chen, Y. Lei, Y. Li, Y. Yu, J. Cai, M.-H. Chiu, R. Rao, Y. Gu, C. Wang, W. Choi, H. Hu, C. Wang, Y. Li, J. Song, J. Zhang, B. Qi, M. Lin, Z. Zhang, A. E. Islam, B. Maruyama, S. Dayeh, L.-J. Li, K. Yang, Y.-H. Lo and S. Xu, Strain Engineering and Epitaxial Stabilization of Halide Perovskites, *Nature*, 2020, **577**(7789), 209–215, DOI: 10.1038/s41586-019-1868-x.

59 A. Franz, D. M. Többens, F. Lehmann, M. Kärgell and S. Schorr, The Influence of Deuteration on the Crystal Structure of Hybrid Halide Perovskites: A Temperature-Dependent Neutron Diffraction Study of $FAPbBr_3$, *Acta Crystallogr., Sect. B: Struct. Sci., Cryst. Eng. Mater.*, 2020, **76**(2), 267–274, DOI: 10.1107/S2052520620002620.

60 X. Ni, L. Lei, Y. Yu, J. Xie, M. Li, S. Yang, M. Wang, J. Liu, H. Zhang and B. Ye, Effect of Br Content on Phase Stability and Performance of $H_2N{=}CHNH_2Pb(I_{1-x}Br_x)_3$ Perovskite Thin Films, *Nanotechnology*, 2019, **30**(16), 165402, DOI: 10.1088/1361-6528/aafeb6.

61 O. Augusto, D. R. Truzzi and E. Linares, Electron Paramagnetic Resonance (EPR) for Investigating Relevant Players of Redox Reactions: Radicals, Metalloproteins and Transition Metal Ions, *Redox Biochemistry and Chemistry*, 2023, **5–6**, 100009, DOI: 10.1016/j.rbc.2023.100009.

62 T. Watanabe, T. Yamanari and K. Marumoto, Deterioration Mechanism of Perovskite Solar Cells by Operando

 © 2025 The Author(s). Published by the Royal Society of Chemistry

Open Access Article. Published on 21 January 2025. Downloaded on 1/22/2026 1:24:09 AM.
This article is licensed under a Creative Commons Attribution-NonCommercial 3.0 Unported Licence.

Observation of Spin States, *Commun. Mater.*, 2020, **1**(1), 96, DOI: 10.1038/s43246-020-00099-7.

63 A. Miyata, A. Mitioglu, P. Plochocka, O. Portugall, J. T.-W. Wang, S. D. Stranks, H. J. Snaith and R. J. Nicholas, Direct Measurement of the Exciton Binding Energy and Effective Masses for Charge Carriers in Organic–Inorganic Tri-Halide Perovskites, *Nat. Phys.*, 2015, **11**(7), 582–587, DOI: 10.1038/nphys3357.

64 K. Galkowski, A. Mitioglu, A. Miyata, P. Plochocka, O. Portugall, G. E. Eperon, J. T.-W. Wang, T. Stergiopoulos, S. D. Stranks, H. J. Snaith and R. J. Nicholas, Determination of the Exciton Binding Energy and Effective Masses for Methylammonium and Formamidinium Lead Tri-Halide Perovskite Semiconductors, *Energy Environ. Sci.*, 2016, **9**(3), 962–970, DOI: 10.1039/C5EE03435C.

65 K. Tanaka, T. Takahashi, T. Ban, T. Kondo, K. Uchida and N. Miura, Comparative Study on the Excitons in Lead-Halide-Based Perovskite-Type Crystals $CH_3NH_3PbBr_3$ $CH_3NH_3PbI_3$, *Solid State Commun.*, 2003, **127**(9), 619–623, DOI: 10.1016/S0038-1098(03)00566-0.

66 M. Hirasawa, T. Ishihara, T. Goto, K. Uchida and N. Miura, Magnetoabsorption of the Lowest Exciton in Perovskite-Type Compound $(CH_3NH_3)PbI_3$, *Phys. B*, 1994, **201**, 427–430, DOI: 10.1016/0921-4526(94)91130-4.

67 Y. Yamada, T. Nakamura, M. Endo, A. Wakamiya and Y. Kanemitsu, Photoelectronic Responses in Solution-Processed Perovskite $CH_3NH_3PbI_3$ Solar Cells Studied by Photoluminescence and Photoabsorption Spectroscopy, *IEEE Journal of Photovoltaics*, 2015, **5**(1), 401–405, DOI: 10.1109/JPHOTOV.2014.2364115.

68 J. Even, L. Pedesseau and C. Katan, Analysis of Multivalley and Multibandgap Absorption and Enhancement of Free Carriers Related to Exciton Screening in Hybrid Perovskites, *J. Phys. Chem. C*, 2014, **118**(22), 11566–11572, DOI: 10.1021/jp503337a.

69 M. R. Tubbs and A. J. Forty, Photographic Applications of Lead Iodide, *Br. J. Appl. Phys.*, 1964, **15**(12), 1553–1558, DOI: 10.1088/0508-3443/15/12/316.

70 A. Abate, D. J. Hollman, J. Teuscher, S. Pathak, R. Avolio, G. D'Errico, G. Vitiello, S. Fantacci and H. J. Snaith, Protic Ionic Liquids as P-Dopant for Organic Hole Transporting Materials and Their Application in High Efficiency Hybrid Solar Cells, *J. Am. Chem. Soc.*, 2013, **135**(36), 13538–13548, DOI: 10.1021/ja406230f.

71 J. Seo, S. Akin, M. Zalibera, M. A. R. Preciado, H. Kim, S. M. Zakeeruddin, J. V. Milić and M. Grätzel, Dopant Engineering for Spiro-OMeTAD Hole-Transporting Materials towards Efficient Perovskite Solar Cells, *Adv. Funct. Mater.*, 2021, **31**(45), 2102124, DOI: 10.1002/adfm.202102124.

72 E. Kasparavicius, M. Franckevičius, V. Malinauskiene, K. Genevičius, V. Getautis and T. Malinauskas, Oxidized Spiro-OMeTAD: Investigation of Stability in Contact with Various Perovskite Compositions, *ACS Appl. Energy Mater.*, 2021, **4**(12), 13696–13705, DOI: 10.1021/acsaem.1c02375.

73 W. Zhang, L. Wang, Y. Guo, B. Zhang, V. Leandri, B. Xu, Z. Li, J. M. Gardner, L. Sun and L. Kloo, Single Crystal Structure and Opto-Electronic Properties of Oxidized Spiro-OMeTAD, *Chem. Commun.*, 2020, **56**(10), 1589–1592, DOI: 10.1039/C9CC09270F.

74 R. S. Sanchez and E. Mas-Marza, Light-Induced Effects on Spiro-OMeTAD Films and Hybrid Lead Halide Perovskite Solar Cells, *Sol. Energy Mater. Sol. Cells*, 2016, **158**, 189–194, DOI: 10.1016/j.solmat.2016.03.024.

75 R. Yekani, H. Wang, P. Ghamari, S. Bessette, J. Sharir-Smith, R. Gauvin and G. P. Demopoulos, Impact of Photo-Induced Doping of Spiro-OMeTAD as HTL on Perovskite Solar Cell Hysteresis Dynamics, *J. Phys. Chem. C*, 2024, **128**(2), 710–722, DOI: 10.1021/acs.jpcc.3c05366.

76 J. Zhang, Q. Daniel, T. Zhang, X. Wen, B. Xu, L. Sun, U. Bach and Y.-B. Cheng, Chemical Dopant Engineering in Hole Transport Layers for Efficient Perovskite Solar Cells: Insight into the Interfacial Recombination, *ACS Nano*, 2018, **12**(10), 10452–10462, DOI: 10.1021/acsnano.8b06062.

77 Y. Yamada, T. Nakamura, M. Endo, A. Wakamiya and Y. Kanemitsu, Photocarrier Recombination Dynamics in Perovskite $CH_3NH_3PbI_3$ for Solar Cell Applications, *J. Am. Chem. Soc.*, 2014, **136**(33), 11610–11613, DOI: 10.1021/ja506624n.